Inductively Coupled Plasma Etching of Bulk, Single-Crystal Ga_2O_3

Running title: Inductively Coupled Plasma Etching of Bulk, Single-Crystal Ga_2O_3
Running Authors: Yang et al.

Jiancheng Yang, Shihyun Ahn and F. Ren

Department of Chemical Engineering, University of Florida, Gainesville FL 32611, USA

S. J. Pearton[a)]

Department of Materials Science and Engineering, University of Florida, Gainesville FL 32611, USA

Rohit Khanna, Kristen Bevlin and Dwarakanath Geerpuram,

Plasma-Therm, Saint Petersburg, FL 33716

A. Kuramata

Tamura Corporation and Novel Crystal Technology, Inc., Sayama Saitama 350-1328, Japan

[a)] Electronic mail: spear@mse.ufl.edu

High ion density dry etching of bulk single-crystal β-Ga_2O_3 was carried out as a function of source power (100-800W), chuck power (15-400W) and frequency (13.56 or 40MHz) in Inductively Coupled Plasma (ICP) systems using Cl_2/Ar or BCl_3/Ar discharges. The highest etch rate achieved was ~1300 Å.min^{-1} using 800W ICP source power and 200W chuck power (13.56MHz) with either Cl_2/Ar or BCl_3/Ar. This is still a

comfortably practical set of conditions, where resist reticulation does not occur because of the effective He backside cooling of the sample in the tool and the avoidance of overly high powers in systems capable of 2000W of source power. The etching is ion-assisted and produces anisotropic pattern transfer. The etched surface may become oxygen-deficient under strong ion-bombardment conditions. Schottky diodes fabricated on these surfaces show increased ideality factors (increasing from 1.00 to 1.29 for high power conditions) and reduced barrier heights (1.1 on reference diodes to 0.86 eV for etched surfaces). This electrically-active damage is dependent on ion energy and flux during the etching. An obvious strategy is to reduce plasma powers toward the end of an etch sequence to reduce the disruption to the Ga_2O_3 surface.

I. INTRODUCTION

There is a strong need to develop high resolution pattern transfer processes for monoclinic Ga_2O_3 because of its emerging role in high power electronics, solar-blind UV photodetectors for fire detection and military surveillance and also gas sensors [1-12]. Ga_2O_3 remains transparent well into the ultraviolet (UV), which allows its use as a transparent conducting oxide in this region of the spectrum [13-18]. To be solar-blind, the deep-UV photodetectors need a cut-off wavelength of 280 nm. With its large direct band gap of ~4.9 eV, Ga_2O_3 also has a very high theoretical breakdown electric field (~8 MV/cm) [19-28]. This means it is of interest for high power electronics in industrial and military applications. A commonly used comparative parameter is the Baliga figure-of-merit for power electronics. This number is almost four times higher for Ga_2O_3 compared to GaN [2,6,9,19]. Reported values of the experimental breakdown field in Ga_2O_3 have reached 3.8

MV/cm, which is higher than the bulk critical field strengths of the more mature GaN and SiC technologies [22]. It is expected that as control of crystal growth and device processing modules improves, the experimental values will move even closer to the theoretical maximum [1,2].

A variety of electronic devices have been reported for Ga_2O_3, including diode rectifiers, metal-semiconductor field-effect transistors (MESFETs), depletion-mode metal-oxide-semiconductor field-effect transistors (MOSFETs) and finfets [19-26] fabricated on either bulk or thin films. In addition, transistors fabricated on exfoliated Ga_2O_3 nanobelts have been shown to exhibit well-behaved dc characteristics such as saturation and transconductance [10,27,28], with associated large values of on-off ratios and stable operation in air.

High quality bulk Ga_2O_3 is now commercially available from several sources [1,14,15] and n-type epi structures are also coming onto the market in limited quantities. There are also significant efforts worldwide to grow more complex epi structures, including heterostructures in the $AlInGaO_x$ system [18], and thus this materials system is poised to make rapid advances in the various device technologies mentioned earlier. However, needs at the moment include the availability of high quality patterning, doping and contacting processes that exist for the more mature semiconductors. Etching is needed for intra-device isolation or for exposing layers for subsequent contacting. While numerous wet etchants have been reported for Ga_2O_3, including HNO_3/HCl, H_2SO_4, H_3PO_4 and HF-based solutions [(29-32)], little is known about its dry etching characteristics and the associated mechanisms and effects on the optical properties of the material [33-35]. Hogan et al. [33] reported etch rates with Cl_2/BCl_3 under conventional reactive ion etching

conditions and BCl_3, BCl_3/SF_6, and CF_4/O_2 under inductively coupled plasma (ICP) conditions. The etch rates were generally low and the resultant surfaces slightly rougher in comparison to those obtained with most compound conducting oxides. Shah and Bhattacharya [35] found no significant temperature dependence of etch rate in BCl_3/Ar or Cl_2/Ar over the range 25-200°C. Plasma-induced damage in Ga_2O_3 is found to increase the conductivity of the near surface and lead to improved n-type Ohmic contact resistivities, as was the case in the early days of GaN technology.

In this paper we report on the dry etching characteristics of high quality bulk Ga_2O_3 using ICP discharges of either Cl_2/Ar or BCl_3/Ar and measure the etch rates, near-surface stoichiometry and electrically-active damage as a function of source and chuck power and also chuck power frequency to understand the nature of the etch mechanism and residual damage. The etching is ion-enhanced and leads to a reduction of Schottky barrier height in diodes fabricated on the etched surfaces.

II. EXPERIMENTAL

The starting sample was a bulk β-phase Ga_2O_3 single crystal with (-201) surface orientation (Tamura Corporation, Japan) grown by the edge-defined film-fed growth method [1]. Hall Effect measurements showed the sample was unintentionally n-type with an electron concentration of ~ 3 x 10^{17} cm^{-3}. Full-area back Ohmic contacts were created using Ti/Au (20nm/80nm) deposited by e-beam evaporation. Photoresist masked and unmasked samples were exposed to $15Cl_2/5Ar$ or 15 $BCl_3/5Ar$ discharges (where the numbers represent the respective gas flows in standard cubic centimeters per minute) in a Plasma-Therm Versaline ICP reactor. The plasma chemistries were chosen based on the

initial reports in the literature and the fact that BCl_3 is a Lewis acid that is effective in reducing oxides. The Cl_2/Ar mixture is a common one for Ga-containing semiconductors such as GaAs and GaN [36]. Since Ga_2O_3 is strongly bonded, ion-assisted etching through Ar ion bombardment is expected to be necessary to achieve practical etch rates We used 3 different configurations that involved either different rf chuck biasing frequency (13.56 or 40MHz) or chuck diameter (6 or 10 inches, which effectively varied the dc self-bias at a fixed power). The 2MHz power applied to the 2000W, 3-turn ICP source was varied from 100-800W, while the rf (13.56 or 40 MHz) chuck power was varied from 15 – 400W (each configuration uses a 600W source). This gave us maximum flexibility in developing high and low etch rate processes and examining the effect of each on near-surface electrical damage and stoichiometry. The source power controls the ion density while the latter controls ion energy. To give some idea of dc self-biases on the sample electrode over the rf power range investigated, this varied from –102V to –820V over the range of conditions used for the Cl_2/Ar etching. For constant 400W ICP, it increased from -146 V at 50W rf power to 820 V at 400W rf power. For a constant 200W rf power, it decreased from -710V at 100W ICP and 200W rf power to -295V at 800W ICP and 200W rf power. Also, for what we will term the low etch rate case, the DC bias voltage was about -102V for 150W ICP and 15W rf power. The electrode setups use mechanical clamping on the periphery of the wafer, with the region between the electrode and wafer back side being enveloped with He (maintaining at least 3.5 torr pressure) sealed behind the wafer to get good heat transfer between the wafer and electrode even at high bias process. Then the heat exchanger temperature of 25°C can be maintained efficiently on the sample helping to prevent any resist reticulation.

Etch rates were obtained from stylus profilometry measurements. Schottky contacts were prepared on the front sides of the unmasked samples by e-beam deposited contacts Ni/Au (20nm/80nm) through a stencil mask. The forward and reverse current-voltage (I-V) [36] characteristics were recorded at 25°C using an Agilent 4145B parameter analyzer. The near-surface stoichiometry was obtained from Auger Electron Spectroscopy (AES) measurements, which was completed at EAG Laboratories, while the anisotropy of etched features were examined by Scanning Electron Microscopy (SEM). The AES system was a Physical Electronics 670 Scanning Auger Microprobe. The electron beam conditions were 10keV, 15nA beam current at 30° from sample normal. For depth profiling, the ion beam conditions were 4 keV Ar^+, 0.8μA, $(3mm)^2$ raster. Figure 1 shows a schematic of the completed diodes.

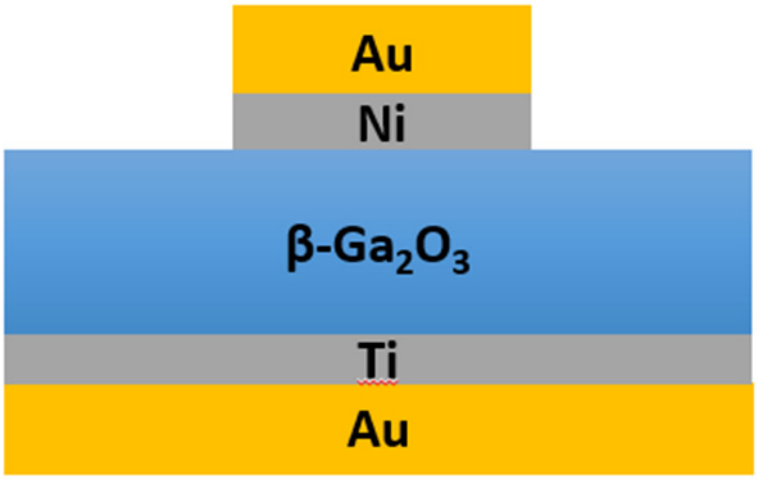

Figure 1. (Color online). Schematics of Ni/Au Schottky diode on the β- Ga_2O_3 substrate.

III. RESULTS AND DISCUSSION

Figure 2 (a) shows the Ga_2O_3 etch rate as a function of ICP source power for the three different configurations and two plasma chemistries. The etch rate increases with

source power as the ion density and reactive neutral density increases and reaches a maximum value of ~1300 Å.min^{-1} using 800W ICP source power and 200W chuck power (13.56MHz) with both Cl_2/Ar and BCl_3/Ar. Shah and Bhattarchya [35] reported the highest dry etch rate to date of 1440 Å. min^{-1} using BCl_3/ Ar on bulk Ga_2O_3, with a selectivity of 2.7 over the SiN_x mask. The use of the BCl_3/Ar in our studies also increases the dc self-bias at a given set of rf and ICP powers. As ICP source power increases, the dc self-bias decreases but the ion density increases and since the etching is ion-assisted, this leads to higher rates. The dc self-biases as a function of source power are shown in Figure 2 (b). Note that the 40MHz rf biasing on the electrode produces very low self-biases and the lowest etch rates. The high rate conditions provide a practical parameter space for mesa formation, where depths up to 1 μm are needed and also does not require such high powers that photoresist reticulation becomes an issue. The fact that BCl_3-based discharges under some conditions can provide higher etch rates than Cl_2-based has been discussed previously [33,35] and may be related to the role of both BCl_3 reacting with the oxygen in the Ga_2O_3 and BCl_2^+ions providing sputtering, while in chlorine-based discharges, the atomic and molecular chlorine species are less effective at removing oxygen.

To demonstrate the effect of rf chuck power on etch rate, Figure 3 (a) shows values as a function of chuck power in the different electrode configurations and the two plasma chemistries. We can obtain a controllable etch rate above 500Å.min^{-1} even at low dc self-biases, with the latter shown in Figure 3 (b). Note that the BCl_3/Ar produces higher self-biases, presumably because of a lower dissociation efficiency compared to Cl_2. The threshold ion energy for the initiation of etching was around 75eV for pure Ar

using the Steinbruchl model [37]. Figure 4 shows the Ga_2O_3 etch rate in both types of plasma chemistry as a function of the substrate bias, V_b. The x-axis is plotted as the square root of the average ion energy, which is the plasma potential of ~25V minus the dc self-bias. The Steinbruchl [37] model is a commonly accepted one for an etching process occurring by ion-enhanced sputtering in a collision-cascade process and predicts the etch rate will be proportional to $E^{0.5}$-$E_{TH}^{0.5}$, where E is the ion energy and E_{TH} is the threshold energy [37]. Therefore, a plot of etch rate versus $E^{0.5}$ should be a straight line with an x-intercept equal to E_{TH}. As mentioned above, in the case of pure Ar, the value of E_{TH} was ~75eV. The BCl_3/Ar data for 13.56 MHz rf power would indicate negative activation energy, but this is an artifact of the complexity of the ion energy distribution in that chemistry, as reported in detail previously [38-40]. The Cl_2/Ar exhibits a threshold energy of ~56 eV, lower than for the pure physical sputtering mode. The fact that Cl_2/Ar exhibits an ion-assisted etch mechanism is consistent with the moderate vapor pressure for the expected group III etch product, $GaCl_3$ (1 Torr at 48°C, melting temperature 78°C [41]) and the high bond strength of Ga_2O_3. To form the etch product, the Ga-O bonds must first be broken by ion bombardment, consistent with the low etch rates for these chemistries. The trends are consistent with the process being an ion-assisted mechanism, which is the case for many compound semiconductors and oxides. We did not have enough data on the 40 MHz rf biasing to draw meaningful conclusions.

One characteristic of ion-assisted etch processes is their high degree of anisotropy because of absence of purely chemical etching component that would lead to undercutting of patterned features. Figure 5 shows SEM micrographs of features etched into the bulk Ga_2O_3 using a Cl_2/Ar discharge and an SiO_2 mask, which is still in place on

the sample. After etching about 3 µm in the case at the top of Figure 5, the sidewalls still have good verticality (as shown in (a)) while the surface (b) shows a small amount of roughening for an etch depth of over 2 µm. Further optimization of etch conditions will almost certainly improve the morphology further.

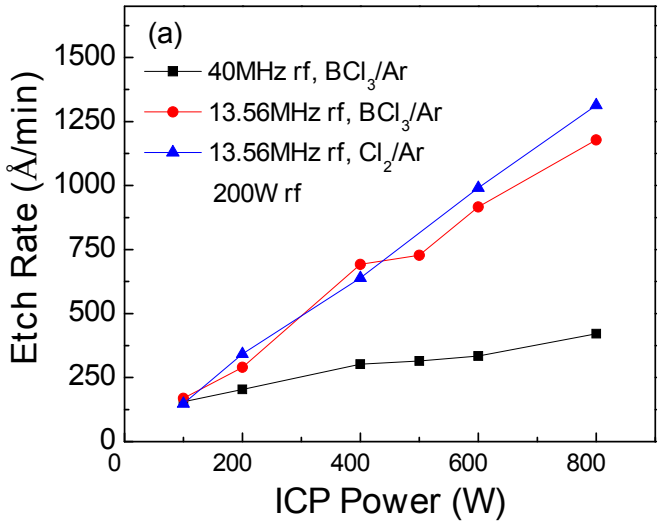

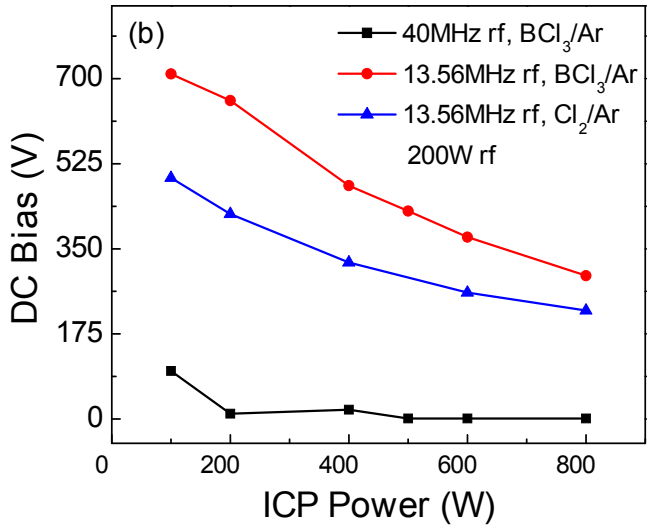

Figure 2. (Color online). (a) β-Ga_2O_3 etch rate as a function of ICP power at constant 200W rf power (13.56MHz) for the three different chamber configurations and the two plasma chemistries. (b) dc self-biases under these conditions.

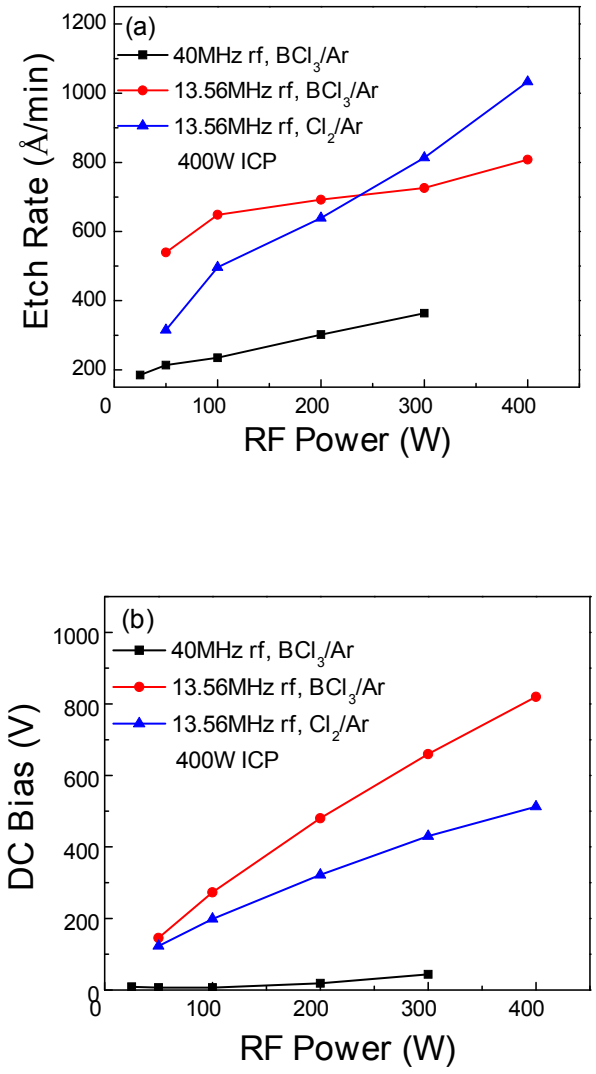

Figure 3. (Color online) (a) β-Ga_2O_3 etch rate as a function of rf power at constant 400W ICP power for the three different chamber configurations and the two plasma chemistries (b) dc self-biases under these conditions.

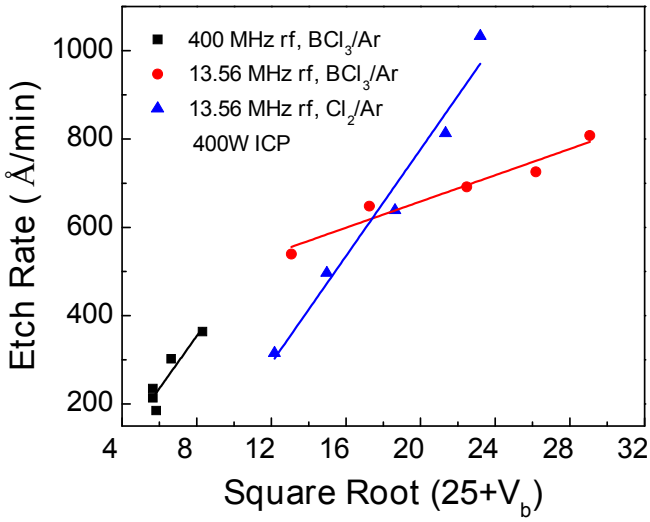

Figure 4. (Color online). Etch rate of Ga_2O_3 in BCl_3/Ar or Cl_2/Ar plasmas as a function of the average ion kinetic energy (plasma potential of +25V minus the measured dc bias voltage) for the three different chamber configurations.

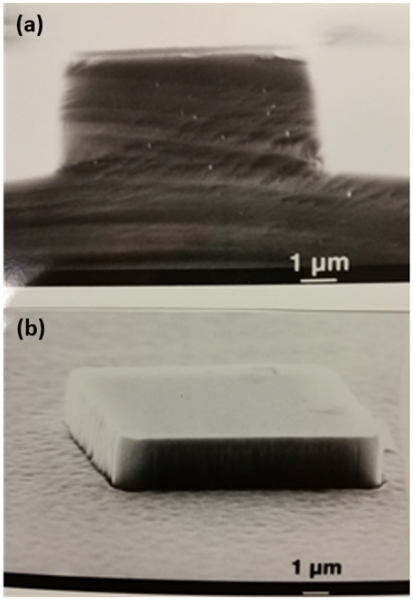

Figure 5. SEM micrographs of bulk Ga_2O_3 dry etched in an ICP discharge of Cl_2/Ar using an SiO_2 mask, which is still in place. The image at top (a) shows the anisotropic nature of

the etching, while the image at bottom (b) shows the surface morphology after an etch depth of over 2μm.

Figure 6 shows the reverse I-V characteristics of diodes fabricated on the etched surfaces using either the 13.56 (a) or 40MHz (b) rf chuck biasing conditions with BCl_3/Ar discharges. The unetched reference diodes showed reverse breakdown voltages of order 50V and this was decreased by the presence of ion-induced damage and non-stoichiometry in the diodes on the dry etched surfaces. The extent of the damage depended on the self-bias, as expected, since the trap states are likely to be point defect complexes. Zhang et al. [43] found five different deep trap states in as-grown Ga_2O_3, ranging in depth from E_C-0.62eV to E_V+0.42 eV.

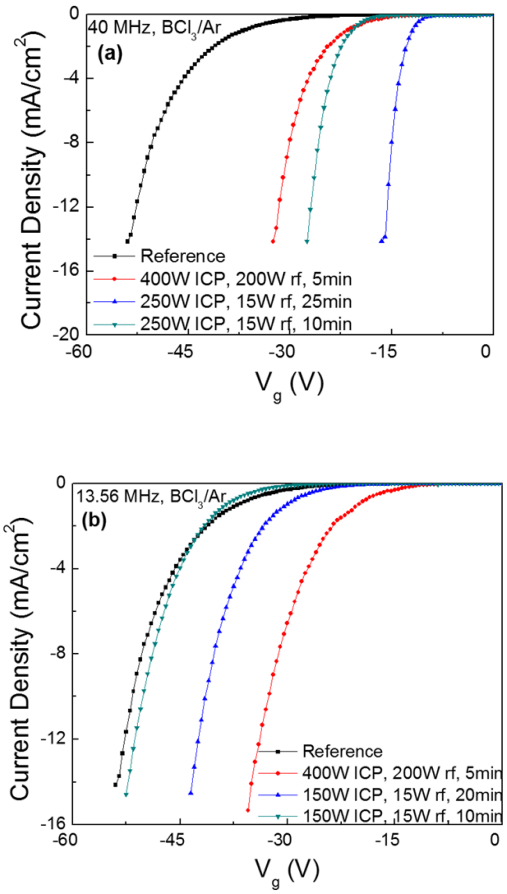

Figure 6. (Color online). Reverse I-V characteristics of diodes fabricated on the etched surfaces using either the 13.56 (top) or 40MHz (bottom) rf chuck biasing conditions with BCl_3/Ar discharges.

The Schottky barrier heights and ideality factors were extracted from the forward I-V characteristics of the type shown in Figure 7 for diodes etched in BCl_3 discharges with 40MHz rf chuck biasing. We obtained this type of data for all the etch configurations and fit the forward I-V characteristics to the relation for the thermionic emission over a barrier [37]

$$J_F = A^*.T^2 \exp(-\frac{e\phi_b}{kT}) \exp(\frac{eV}{nkT}) \qquad (1)$$

where J is the current density, A^* is the Richardson's constant for n-GaN, T the absolute temperature, e the electronic charge, ϕ_b the barrier height, k Boltzmann's constant, n the ideality factor and V the applied voltage. We did this for the high and low etch rate conditions for each of the three reactor configurations and the results are shown in Figure 8. The Schottky diodes fabricated on these surfaces show increased ideality factors (increasing from 1.00 to a worst-case of 1.29 for high power conditions) and reduced barrier heights (1.1 on reference diodes to a worst-case of 0.86 eV for etched surfaces). Note that the amount of degradation in the barrier height from the reference values is a function of etch time under low etch rate conditions, indicating that longer times allow the damage to accumulate under these conditions and also that the frequency of the rf chuck bias plays a strong role through its influence on chuck dc self-bias and hence incident ion energy. Table 1 also shows a summary of the etch rates, barrier heights and ideality factors for Ga_2O_3 etched in the three different configurations of the etch tools.

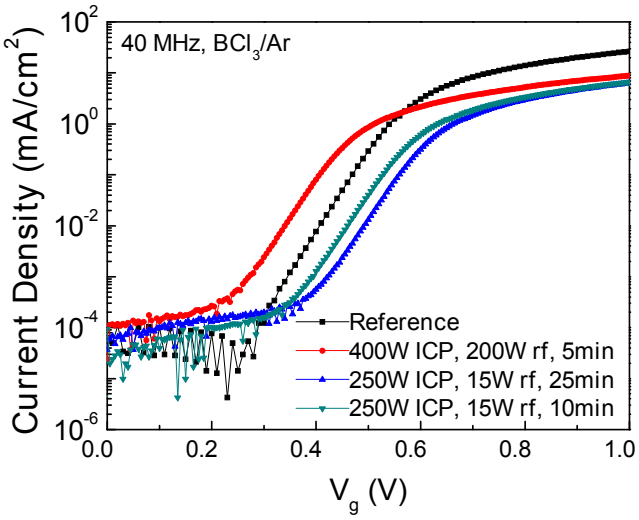

Figure 7. (Color online). Forward I-V characteristics for diodes etched in BCl_3 /Ar discharges with 40MHz rf chuck biasing.

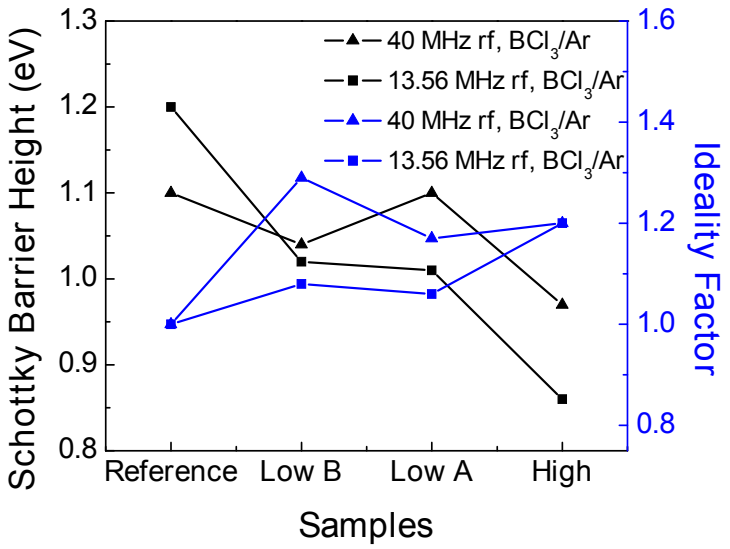

Figure 8. (Color online). Schottky barrier height and ideality factor for diodes etched at high and low etch rate conditions shown in Table 1.

Note that the usual procedures for eliminating the near-surface damage region of dry etched semiconductors include either annealing or a wet etch clean-up [44-47]. The wet etching under these conditions in wide bandgap materials can often be self-limiting because only the damaged region etches at a significant rate. Such annealing and shallow wet etch processes still need to be developed for Ga_2O_3.

Table 1. Summary of etch rates, barrier heights and ideality factors as a function of ICP power and also rf chuck power and frequency. The etch rate data for high rate, low rate A, and low rate B was obtained for 5 min, 10 min, and 25 min, respectively.

Sample/Plasma chemistry	Rf Power Frequency (MHz)	Rf Power (W)	ICP Power (W)	DC Self-Bias (-V)	Etch Rate (Å/min)	Schottky Barrier Height (eV)	Ideality Factor
Reference		0	0	0	0	1.20	1.00
High Etch Rate- BCl_3/Ar	13.56 MHz	200	400	480	692	0.86	1.20
Low Etch Rate A- BCl_3/Ar	13.56 MHz	15	150	102	121	1.01	1.06
Low Etch Rate B- BCl_3/Ar	13.56 MHz	15	150	102	121	1.02	1.08
High Etch Rate- BCl_3/Ar	40MHz	200	400	19	302	0.97	1.20
Low Etch Rate A- BCl_3/Ar	40MHz	15	250	4	27	1.10	1.17
Low Etch Rate B- BCl_3/Ar	40MHz	15	250	4	27	1.04	1.29

High Etch Rate- Cl_2/Ar	13.56 MHz	400 (small electrode)	400	547	173	0.89	1.69
Low Etch Rate A- Cl_2/Ar	13.56 MHz	15 (small electrode)	100	76	15	1.02	1.11
Low Etch Rate B- Cl_2/Ar	13.56 MHz	15 (small electrode)	100	76	15	1.01	1.15

The near-surface composition of the samples was measured by AES depth profiling. Figure 9 shows the data for the low (a) and high (b) etch rate conditions of rows 2 and 3 from Table I. Within the experimental error, there was no significant change in O/Ga ratio in this region relative to the unetched control samples (Figure 10), indicating that the disruption to the surface is not sufficient to be detected by chemical analysis techniques but is present to a level that it changes the electrical properties (Schottky barrier height and ideality factor). In our experience, this indicative of a nearly-optimized process, ie. the damage is at a small enough level that it should be relatively simple to use the annealing or wet-etch clean-up steps to remove this affected region. When nitride or oxide semiconductors are dry etched under non-optimized conditions, it is common to note a preferential loss of the nitrogen or oxygen from the surface, leading in general to highly conducting layers [(48)].

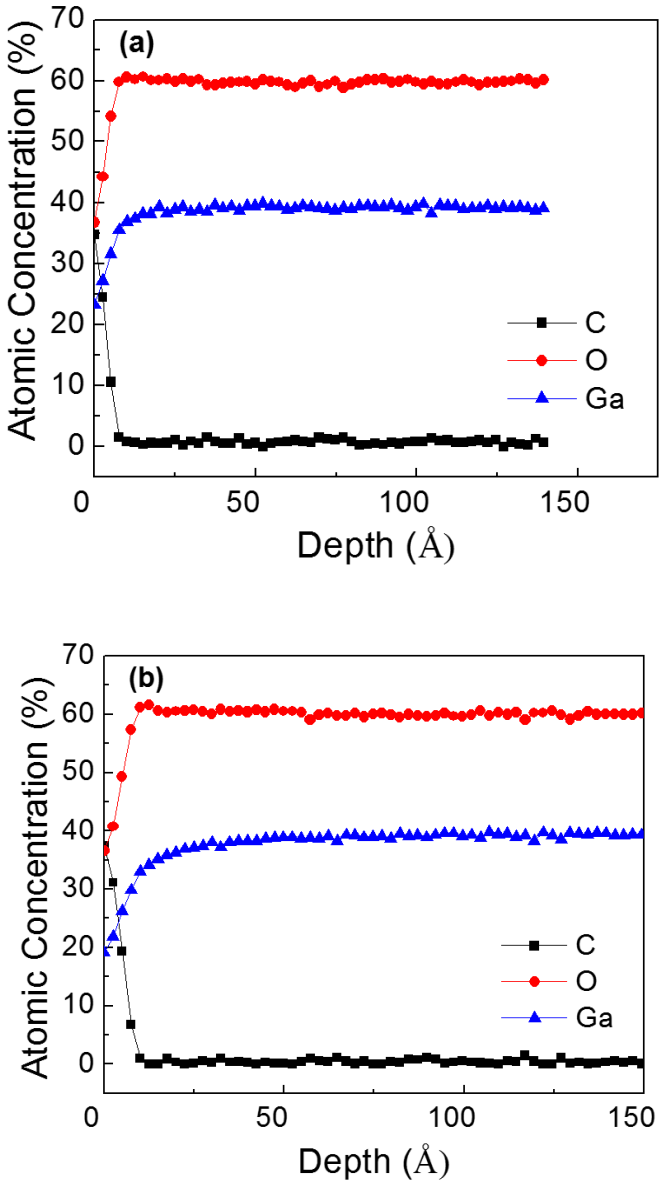

Figure 9. (Color online). AES depth profiles of Ga_2O_3 surfaces before and after either low rate (a) or high rate (b) etching in BCl_3/Ar discharges. The etch conditions correspond to rows 2 and 3 of Table I.

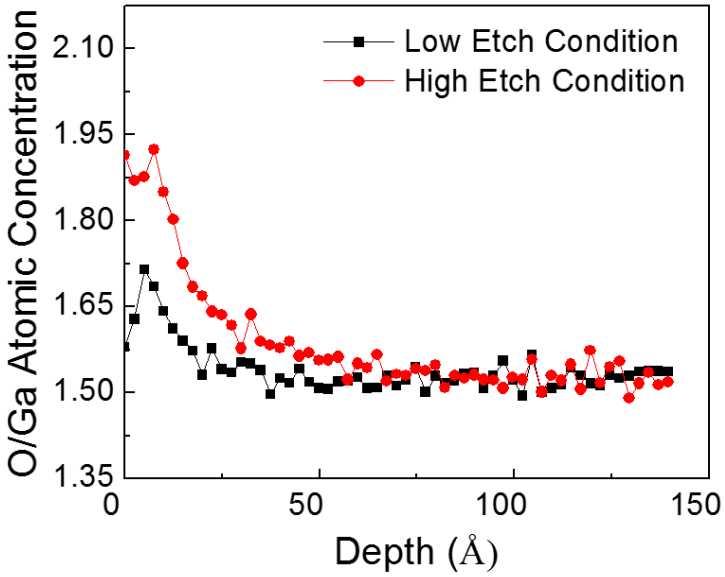

Figure 10. (Color online). O/Ga ratio obtained from AES depth profiles of Ga_2O_3 near surface region after etching in BCl_3/Ar discharges. The etch conditions correspond to rows 2 and 3 of Table I.

IV. SUMMARY AND CONCLUSIONS

In conclusion, we have investigated the etch mechanism for Ga_2O_3 in plasma chemistries of BCl_3/Ar and Cl_2 /Ar. For both chemistries, the etch rate increases with ion energy as predicted from an ion-assisted chemical sputtering process. Both chemistries give similar maximum rates under ICP conditions. Both high rate and low rate processes have been developed for applications that need either higher rates for deep mesa formation or finer control for adjustment of threshold voltage in gate-recessed transistor structures. Anisotropic features can be created to depths of several microns with these processes and simple masks. The near-surface stoichiometry changes as a result of dry etching are enough to reduce the barrier height and increase the ideality factors on

Schottky diodes fabricated on these surfaces, but are not significant enough to be detected by AES.

ACKNOWLEDGMENTS

The project or effort depicted was also sponsored by the Department of the Defense, Defense Threat Reduction Agency, HDTRA1-17-1-011, monitored by Jacob Calkins. The content of the information does not necessarily reflect the position or the policy of the federal government, and no official endorsement should be inferred. Part of the work at Tamura was supported by "The research and development project for innovation technique of energy conservation" of the New Energy and Industrial Technology Development Organization (NEDO), Japan. We also thank Dr. Kohei Sasaki from Tamura Corporation for fruitful discussions.

[1] Akito Kuramata, Kimiyoshi Koshi, Shinya Watanabe, Yu Yamaoka, Takekazu Masui, and Shigenobu Yamakoshi, Jpn. J. Appl. Phys. **55**, 1202A2 (2016).

[2] M.J. Tadjer, M.A. Mastro, N.A. Mahadik, M. Currie, V.D. Wheeler, J.A. Freitas, Jr., J.D. Greenlee, J.K. Hite, K.D. Hobart, C.R. Eddy, Jr. and F.J. Kub, J. Electr. Mater. **45**, 2031 (2016).

[3] Masataka Higashiwaki, Keita Konishi, Kohei Sasaki, Ken Goto, Kazushiro Nomura, Quang Tu Thieu, Rie Togashi, Hisashi Murakami, Yoshinao Kumagai, Bo Monemar, Akinori Koukitu, Akito Kuramata, and Shigenobu Yamakoshi, Appl. Phys. Lett. **108**, 133503 (2016)

[4]K. Sasaki, M. Higashiwaki, A. Kuramata, T. Masui, and S. Yamakoshi, Appl. Phys. Express **6**, 086502 (2013).

[5]Zhi Guo, Amit Verma, Xufei Wu, Fangyuan Sun, Austin Hickman, Takekazu Masui, Akito Kuramata, Masataka Higashiwaki, Debdeep Jena, and Tengfei Luo, Appl. Phys. Lett. **106**, 111909 (2015).

[6]M. Higashiwaki, K. Sasaki, A. Kuramata, T. Masui, and S. Yamakoshi, Phys. Status Solidi B, **211**, 21 (2014).

[7]O. Ueda, N. Ikenaga, K. Koshi, K. Iizuka, A. Kuramata, K. Hanada, T. Moribayashi, S. Yamakoshi, and M. Kasu, Jpn. J. Appl. Phys. **55**, 1202BD (2016).

[8]S. I. Stepanov, V. I. Nikolaev, V. E. Bougrov, and A. E. Romanov, Rev. Adv. Mater. Sci., **44**, 63 (2016)

[9]Marko J. Tadjer, Nadeemullah A. Mahadik, Virginia D. Wheeler, Evan R. Glaser, Laura Ruppalt, Andrew D. Koehler, Karl D. Hobart, Charles R. Eddy, Jr., and Fritz J. Kub, ECS J. Solid State Sci. Technol. **5**, 468 (2016).

[10]Janghyuk Kim, Sooyeoun Oh, Michael Mastro and Jihyun Kim, Phys. Chem. Chem Phys. **18**, 15760 (2016).

[11]R. Pandeeswari, B.G. Jeyaprakash, Sensors and Actuators B: Chemical, **195**, 206 (2014)

[12]A.M Armstrong, M.H. Crawford, A. Jayawardena, A. Ahyi and S. Dhar, J. Appl. Phys., **119**, 103102 (2016).

[13]Man Hoi Wong, Kohei Sasaki, Akito Kuramata, Shigenobu Yamakoshi, and Masataka Higashiwaki, Appl. Phys. Lett. **106**, 032105 (2015)

[14]K. Hoshikawa, E. Ohba, T. Kobayashi, J. Yanagisawa, C. Miyagawa, Y. Nakamura, J. Crystal Growth, **447**, 36 (2016).

[15]Z. Galazka, R. Uecker, D. Klimm, K. Irmscher, M. Naumann, M. Pietsch, A. Kwasniewski, R. Bertram, S. Ganschow, and M. Bickermann, ECS J. Solid State Sci. Technol., **6**, Q3007 (2017).

[16]Michele Baldini, Martin Albrecht, Andreas Fiedler, Klaus Irmscher, Robert Schewski, and Günter Wagner, ECS J. Solid State Sci. Technol. **6**, Q3040 (2017).

[17]S. Rafique, L. Han, M.J. Tadjer, J.A. Freitas Jr, N.A. Mahadik and H. Zhao, Appl. Phys. Lett. **108**, 182105(2016).

[18]S. W. Kaun, F. Wu, and James S. Speck, J. Vac. Sci. Technol. A33, 041508 (2015).

[19]M. Higashiwaki, K. Sasaki, H. Murakami, Y. Kumagai, A. Koukitu, A. Kuramata, T. Masui and S. Yamakosh, Semicond. Sci. Tech., **31**, 034001 (2016).

[20]Masataka Higashiwaki, Kohei Sasaki, Akito Kuramata, Takekazu Masui, and Shigenobu Yamakoshi, Appl. Phys. Lett. **100**, 013504 (2012).

[21]K. D. Chabak, N. Moser, A. J. Green, D. E. Walker Jr., S. E. Tetlak, E. Heller, A. Crespo, R. Fitch, J. P. McCandless, K. Leedy, M. Baldini, G. Wagner, Z. Galazka, X. Li and G. Jessen, Appl. Phys. Lett. **109**, 213501 (2016.)

[22]A. J. Green, K. D. Chabak, E. R. Heller, R. C. Fitch, Jr., M. Baldini, A. Fiedler, K. Irmscher, G. Wagner, Z. Galazka, S. E. Tetlak, A. Crespo, K. Leedy and G. H. Jessen, IEEE Electr. Device L. **37**, 902 (2016).

[23]M.H. Wong, K. Sasaki, A. Kuramata, S. Yamakoshi and M. Higashiwaki, IEEE Electr. Device L., **37**, 212 (2016).

[24]K. Sasaki, M. Higashiwaki, A. Kuramata, T. Masui, and S. Yamakoshi, IEEE Electron. Dev. Lett., **34**, 493 (2013).
[25]Man Hoi Wong, Kohei Sasaki, Akito Kuramata, Shigenobu Yamakoshi and Masataka Higashiwaki, Appl. Phys. Lett. **106**, 032105 (2015).
[26]S. Oh, G. Yang, and Jihyun Kim, ECS J. Solid State Sci. Technol. **6**, Q3022 (2017).
[27]W. S. Hwang, A. Verma, H. Peelaers, V. Protasenko, S. Ruvimov, H.(Grace) Xing, A. Seabaugh, W. Haensch, C. Van de Walle, Z. Galazka, M. Albrecht, R. Fornari and D. Jena, Appl. Phys. Lett. **104**, 203111 (2014).
[28]Shihyun Ahn, Fan Ren, Janghyuk Kim, Sooyeoun Oh, Jihyun Kim, Michael A. Mastro and S. J. Pearton, Appl. Phys. Lett.**109**, 062102 (2016).
[29]Shigeo Ohira and Naoki Arai, Phys. Status Solidi C **5**, 3116 (2008).
[30]T. Oshima, T. Okuno, N. Arai, Y. Kobayashi and S. Fujita, Jpn. J. Appl. Phys. **48**, 040208 (2009).
[31]M. Passlack, E. F. Schubert, W. S. Hobson, M. Hong, N. Moriya, S. N. G. Chu, K. Konstadinidis, J. P. Mannaerts, M. L. Schnoes, and G. J. Zydzik, J. Appl. Phys. **77**, 686 (1995).
[32] F. Ren, M. Hong, J. P. Mannaerts, J. R. Lothian, and A. Y. Cho, J. Electrochem. Soc. **144**, L239 (1997).
[33]Jack E Hogan, Stephen W Kaun, Elaheh Ahmadi, Yuichi Oshima and James S Speck, Semicond Sci. Tech.**31**, 065006 (2016).
[34]H. Liang, Y. Chen, X. Xia, C. Zhang, R. Shen, Y. Liu, Y. Luo and G. Du, Mat. Sci. Semicond. Proc. **39**, 582 (2015)
[35]Amit P. Shah and Arnab Bhattacharya (submitted to JVST-A)
[36]R.J. Shul, M.C. Lovejoy, A.G. Baca, J.C. Zolper, D.J. Rieger, M.J. Hafich, R.F. Corless and C.B. Vartuli, J. Vac. Sci Technol. **A13** 912 (1995).
[37]D. K. Schroder, Semiconductor Material and Device Characterization, (Wiley and Sons, NY 1990).
[38]C. Steinbruchel, Appl. Phys. Lett. 55**,** 1960 (1989).
[39]K. Pelhos, V.M. Donnelly, A. Kornblit, M.L. Green, R.B. Van Dover, L. Manchanda and E. Bower, J. Vac. Sci. Technol. **A19** 1361 (2001).
[40]C.C. Chang, K.V. Guinn, V.M. Donnelly and I.P. Herman, J. Vac. Sci. Technol. **A13** 1970 (1995).
[41]K. Ip, K. Baik, M.E. Overberg, E.S. Lambers, Y.W. Heo, D.P. Norton, S.J. Pearton, F. Ren and J.M. Zavada, Appl. Phys. Lett. **81**, 3546 (2002).

[42]C Bernard, C Chatillon, A. Ait-Hou, R Hillel, Y Monteil, J Bouix, J. Chem. Thermodynam., **20**, 129 (1988).

[43]Z. Zhang, E. Farzana, A. R. Arehart, and S. A. Ringel, Appl. Phys. Lett. **108**, 052105 (2016).

[44]A. G. Baca, A. M. Armstrong, A. A. Allerman, E. A. Douglas, C. A. Sanchez, M. P. King, M. E. Coltrin, T. R. Fortune and R. J. Kaplar, Appl. Phys. Lett. **109**, 033509 (2016).

[45]X.A. Cao, S.J. Pearton, A.P. Zhang, G.T. Dang, F. Ren, R.J. Shul, L. Zhang, R. Hickman and J.M. Van Hove, Appl. Phys. Lett.**75**, 2569 (1999).

[46]Erica A. Douglas, Carlos A. Sanchez, Robert J. Kaplar, Andrew A. Allerman and Albert G. Baca, J. Vac. Sci. Technol. A **35**, 021305 (2017).

[47]X.A. Cao, H. Cho, S.J. Pearton, G.T. Dang, A.P. Zhang, F. Ren, R.J. Shul, L. Zhang, R. Hickman and J.M. Van Hove, Appl. Phys. Lett.**75**, 232 (1999).

[48]See, for example, S.W. Pang, Chapter 8 in Handbook of Advanced Plasma Processing Techniques, ed. R.J. Shul and S.J. Pearton (Springer, Berlin, 2000).